Intermittency of quantum turbulence with superfluid fractions from 0% to 96%

E. Rusaouen, B. Chabaud, J. Salort, and P.-E. Roche

Citation: Physics of Fluids **29**, 105108 (2017); doi: 10.1063/1.4991558
View online: http://dx.doi.org/10.1063/1.4991558
View Table of Contents: http://aip.scitation.org/toc/phf/29/10
Published by the American Institute of Physics

Intermittency of quantum turbulence with superfluid fractions from 0% to 96%

E. Rusaouen,[1] B. Chabaud,[1] J. Salort,[2] and P.-E. Roche[1]
[1]*University of Grenoble Alpes, CNRS, Grenoble INP, Institut Néel, 38000 Grenoble, France*
[2]*University of Lyon, Ens de Lyon, University Claude Bernard, CNRS, Laboratoire de Physique, F-69342 Lyon, France*

(Received 21 June 2017; accepted 30 September 2017; published online 23 October 2017)

The intermittency of turbulent superfluid helium is explored systematically in a steady wake flow from 1.28 K up to $T > 2.18$ K using a local anemometer. This temperature range spans relative densities of superfluids from 96% down to 0%, allowing us to test numerical predictions of enhancement or depletion of intermittency at intermediate superfluid fractions. Using the so-called extended self-similarity method, scaling exponents of structure functions have been calculated. No evidence of temperature dependence is found on these scaling exponents in the upper part of the inertial cascade, where turbulence is well developed and fully resolved by the probe. This result supports the picture of a profound analogy between classical and quantum turbulence in their inertial range, including the violation of self-similarities associated with inertial-range intermittency. *Published by AIP Publishing.*
https://doi.org/10.1063/1.4991558

I. MOTIVATION AND STATE-OF-THE-ART

A. Introduction

When liquid ^{4}He is cooled below $T_\lambda \simeq 2.18$ K, it experiences a phase transition and enters a superfluid state, called He-II. The hydrodynamics of superfluids has fascinated physicists and engineers since the late 1930s, in particular for their ability to flow without experiencing any viscosity, and for the quantification of vorticity, discovered a decade later.[1,2] Due to their exotic properties, He-II and other quantum fluids have also attracted interest from the classical turbulence community, as it allows tackling some open problems using a fluid with unique dissipative and vorticity properties.[3] The so-called *quantum turbulence* of mechanically stirred He-II was found to share many features with classical turbulence,[4] in particular in the so-called *inertial range* of scales, where the kinetic energy continuously cascades from larger to smaller eddies,[5] resulting in a Kolmogorov-Obhukov-like $k^{-5/3}$ velocity power spectrum (k is the wavenumber). The present study explores the phenomenon of intermittency in this inertial range, an effect associated with a violation of self-similarity of velocity fluctuations, which is still actively studied in classical turbulence.[6–9]

Using the Landau and Tisza two-fluid model, He-II hydrodynamics can be described by two interpenetrating fluids in mutual interaction: one inviscid *superfluid* of density ρ_s and one *normal fluid* of viscosity μ and density $\rho_n = \rho - \rho_s$ (where ρ is the density of He-II).[1,2] By changing the temperature between T_λ and 0 K, the superfluid fraction ρ_s/ρ can be arbitrarily chosen between 0% and 100%. This temperature dependence is a key property of the present study: it allows exploring intermittency from the Navier-Stokes case ($T > T_\lambda$ and $\rho_s/\rho = 0\%$), down to a nearly pure superfluid (here $\rho_s/\rho \simeq 96\%$). The universality of intermittency can therefore be tested versus a continuous change of fluid properties.

B. Contradictory numerical predictions

For convenience, Table I summarizes the literature review presented in the following paragraph.

The first experimental studies of intermittency in superfluids were published in 1998 and 2011.[10,11] They focused on the low temperature regime with superfluid fractions $\rho_s/\rho = 92\%$ and 85% (respectively, 1.4 K and 1.56 K). Both experiments reported no difference with the intermittency of classical fluids.

In 2011, some direct numerical simulations (DNSs) based on the so-called HVBK (Hall-Vinen-Bekharevich-Khalatnikov) continuous model[1,2] were also reported in Ref. 11. In the HVBK model, the quantized nature of the superfluid vorticity is coarse-grained into a continuous field, which allows describing the fluid using an Euler equation (for the superfluid) and a Navier-Stokes term (for the normal fluid) coupled by a mutual friction term. In the DNS study mentioned above, both the low and high temperature regimes were explored, with superfluid fractions of 98% and 9%, respectively. Again no difference was found with the classical fluid intermittency.

In 2013, Boué *et al.*[12] reported numerical simulations using a shell-model[13] of the HVBK dynamics. In the low and high temperature limits, they found the same results as the previous studies. But they also reported a significant *enhancement* of intermittency at intermediate temperatures, corresponding to the window $\rho_s/\rho \simeq 20\% - 90\%$ (yet the exponent of the second order structure function reaches values corresponding to the absence of intermittency).[12] In 2016, numerical studies by Shukla and Pandit[14] using a different variant of shell model [respectively, Sabra version and a GOY (Gledzer-Ohkitani-Yamada) variant] agreed on the low and high temperature limits but reported opposite results in the intermediate window with a significant *reduction* or

TABLE I. Experimental and numerical studies of quantum turbulence intermittency. The statements "more" or "less" intermittent are based on structure functions of order larger than two (e.g., as shown in Fig. 11). The second order structure function can suggest an opposite trend.

References	Approach	Superfluid fraction ρ_s/ρ (%)	Intermittency exponents ($\zeta_{p\geq 3}$)
Maurer and Tabeling[10]	Experiment	92	Consistent with classical
Salort *et al.*[11]	Experiment	0 and 85	Consistent with classical
	DNSs (based on HVBK)	9 and 98	Consistent with classical
Boué *et al.*[12]	Shell-model simulations	~20 – 90	*More intermittent*
	(Based on HVBK)	$\lesssim$20 or $\gtrsim$90	Consistent with classical
Shukla and Pandit[14]	Shell-model simulations	~10 – 80	*Less intermittent*
	(Based on HVBK)	$\lesssim$40 or $\gtrsim$65	Consistent with classical
Bakhtaoui and Merahi[15]	LES simulations	84	*More intermittent*
	(Based on HVBK)	23 and 98	Consistent with classical
Krstulovic[16]	Gross-Pitaevskii simulation	100	*More intermittent*
Rusaouen *et al.*[17]	Experiment	0, 19, and 81	Consistent with classical
Rusaouen *et al.* (present study)	Experiment	0, 11.3, 51, 63, 85.8, and 95.7	Consistent with classical

absence of intermittency (the second order structure function exhibits a more complex behavior). No experimental data were available for comparison in this intermediate temperature range.

In 2014, some Large Eddy Simulations (LESs) of the HVBK model were reported for ρ_s/ρ = 98%, 84%, and 23% by Bakhtaoui and Merahi.[15] The authors report a significant difference of intermittent behavior at their intermediate temperature (T = 1.6 K, ρ_s/ρ = 84%) compared to their lowest and highest temperature cases, and they interpret it as a signature of intermittency *enhancement*.

Adding to the apparent puzzle, another 2016 study explored quantum-fluid intermittency at zero temperature (ρ_s/ρ = 100%) using Gross-Pitaevskii equations and concluded on intermittency *enhancement*.[16] Once again, no experimental data on intermittency are available today in this zero temperature case where the normal fluid fraction is null.

Finally, a 2017 experimental study in a highly turbulent von Kármán cell ($R_\lambda \sim 10\,000$) took a different perspective by analyzing the intermittent statistics of coherent structures for ρ_s/ρ = 0%, 19%, and 81% (±2%). No temperature dependence was found,[17] like in the previous experimental studies.

As a side note, we can mention for completeness two ongoing studies have been reported by Emil Varga and Victor L'vov in the Quantum Turbulence workshop held in Tallahassee in April 2017: one experimental work on transverse structure functions performed in Tallahassee and numerical simulations performed by DNS in collaboration between groups from Rehovot and Rome. Some DNSs using the HVBK model have also been performed lately in Rahul Pandit's group (private communication).

The puzzle of these contradictory numerical results and the lack of experimental data at intermediate temperatures motivated the present systematic experiment.

C. Methodology

Our experimental aim is a high-resolution assessment of the temperature-dependence of intermittency in the inertial range of turbulent helium from its classical state ($T > T_\lambda$) to its superfluid one, down to the temperature corresponding to a superfluid fraction of ρ_s/ρ = 96%.

An accurate determination of intermittency is only possible under several conditions. One condition is a good convergence of velocity statistics, which led to the choice of a steady flow rather than an unsteady one. The second condition is to have a sufficiently large inertial range,[18] and the third condition is to resolve its velocity fluctuations: here we cover more than 1.5 decades of frequencies, as illustrated in Fig. 6.

After considering different types of flows, such as the grid and von Kármán flow, we chose to study the turbulence in the wake of a disc. Furthermore, the flow was confined in a pipe to preserve a well-defined mean direction. Although wake turbulence is neither isotropic nor homogeneous, it appeared as a good compromise to meet the requirements listed above and to explore the temperature dependence of intermittency in a well-defined developed turbulent flow. Wakes of discs have been widely studied in classical turbulence (e.g., Refs. 19–22), and even in superfluid helium for one of the intermittency studies previously mentioned.[11] Thus, the existing literature allows us to size the experiment (see Sec. II A) and probes (see Sec. II B) in order to generate a well-defined turbulent flow (see Sec. III A).

Compared to the previous experimental studies,[10,11] the flow temperature is varied systematically and over a broader range. Reference measurements are performed above and below the superfluid transition in conditions as similar as possible, to allow one-to-one comparison. To allow a direct comparison with the previous studies cited above, intermittency is quantified by the exponents of the velocity structure functions, as discussed later (Sec. III B).

II. THE TOUPIE EXPERIMENT

A. Experimental setup

The TOUPIE liquid helium wind-tunnel, previously described in Ref. 5, has been upgraded and adapted to the requirements of the experiment. It consists in a 1-m-long wind-tunnel, mounted at the bottom end of a cryogenic insert exceeding 2 m in length [see Fig. 1(a)]. Such a long insert allows an

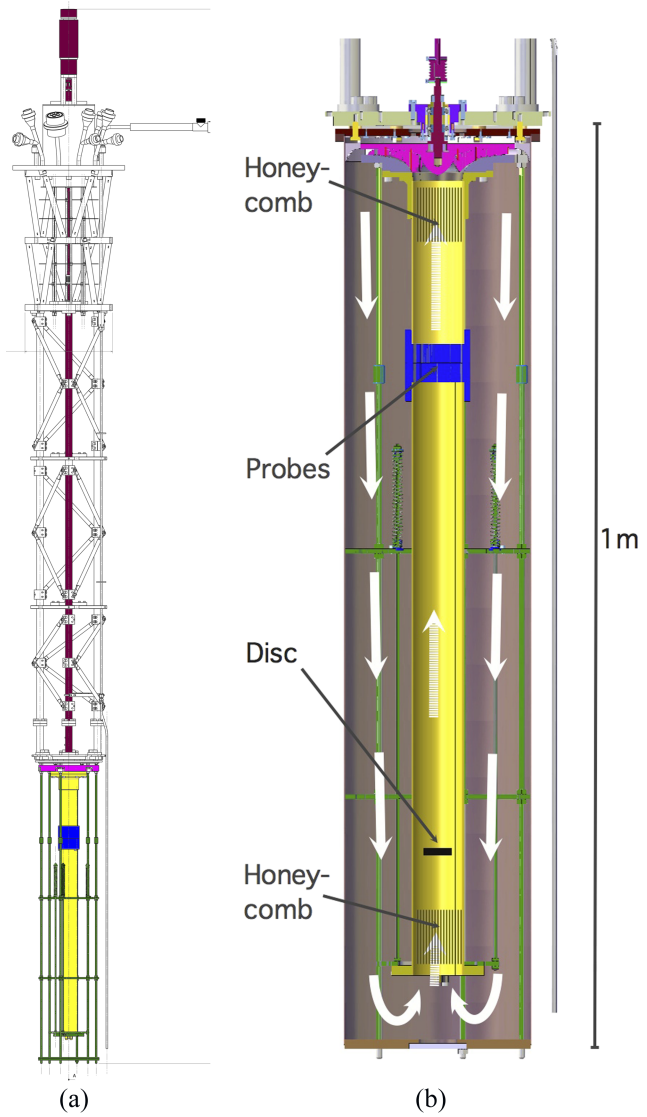

FIG. 1. The TOUPIE experiment: yellow part is the inner wind tunnel, blue part is the instrumentation support, green tends for the decoupling springs, and the wake-generator disc is in black. The room temperature motor and drive shaft are schematized in violet and the propeller is in pink. (image © Ph.R.). (a) General view. (b) Zoom on the wind tunnel part.

hydrostatic pressurization of the wind tunnel under a column of liquid helium exceeding $h = 1$ m in height, which prevents cavitation up to flow velocities exceeding $\sqrt{2gh} \simeq 4.4$ m/s. The insert is designed to provide high stiffness to the experiment thanks to the truss structure visible on the general view in Fig. 1(a).

The wind-tunnel itself has a coaxial cylindrical geometry: the test section is within the inner cylinder, while the return channel is between the inner and outer cylinders [see Fig. 1(b)]. The 19.5-cm-diameter outer cylinder is made of a thin Cu sheet for efficient energy exchange with the surrounding cooling helium bath, while the inner cylinder is a 80 cm-long and 5.1 cm-internal-diameter cardboard tube (in yellow on the sketch). Cardboard is chosen to reduce the propagation of vibrations. It is partly decoupled from the rest of the structure by three springs (in green on the sketch). The cardboard tube (from the roll of a poster-printer paper) is interrupted by a massive brass ring at the location where the probes are mounted (in blue on the sketch). The spring stiffness is chosen just as large as required to support slightly more the weight of the brass ring and tube ($\simeq$1.5 kg). This allows benefiting from the low-pass filter of this mass-spring mechanical resonator.

Reminiscent of the design of the so-called *étoile flow conditioner*, six flow-guides made of Kapton sheets prevent helicoidal motion of the flow along the return section. In the same spirit, two honeycombs are inserted at the entrance of the inner pipe and at its end, right upstream the propeller. Both honeycombs exhibit the same cell density: 10 cells/cm^2 and respective length of 5 cm (input of the wind-tunnel) and 2 cm (output of the wind-tunnel). Their main purpose is to straighten the flow, remove swirl, and lower to turbulence intensity.[23]

Flow instabilities sustain an acoustic standing wave settling in helium, between the top and bottom walls of the wind-tunnel. To reduce its impact on the Pitot tube measurement (see Subsection II B), the probe-holding brass ring was initially located at mid-height in the tunnel, where the 1st mode of the standing wave has a pressure node. The improvement on the acoustic pollution captured by the Pitot tube was found marginal and this probe-positioning constrain was abandoned.

The fluid is set into motion by a centrifugal pump optimized to reach a mass flow of 130 g/s of liquid helium. A drive shaft connects the pump to a motor at ambient temperature. Special attention was paid to the stainless steel ball bearing located at the bottom of the shaft since past experiments have shown that it can be a source of vibrations in the few hundreds of Hz range. For cost reasons, we use standard stainless steal bearings, cleaned in a solvent to remove the lubricant oil which would freeze at low temperatures. Unsurprisingly, these oil-free bearings aged more rapidly, even when dry lubricants are added, which result in more vibrations. As a consequence, a new bearing is mounted before each cool-down of the wind-tunnel. To spoil the acoustic impedance matching coupling between the stainless steal bearing and the stainless steal plate on which it is fixed, a fiber-glass-reinforced epoxy cage in inserted in-between [in purple on Fig. 1(b)].

Rotation of the shaft (Ω in Hz) is measured using a dynamo and is proportional to the velocity of the fluid V in the test-section, up to small corrections due a reduced efficiency of the pump at the lowest rotation frequencies. Unfortunately, the proportionality coefficient—around few tens of Hz/(m s^{-1})—was not measured accurately due to a technical problem. So velocity is kept in arbitrary units of propeller rotation.

A disc of diameter $d = 25.5$ mm, 3.7 mm thickness with sharp edges generates a turbulent wake in the test section. For the maximum He mass flow of 130 g/s and a density of $\rho = 145$ kg/m^3, the wind-tunnel has been designed to reach a maximum mean velocity which is $\langle V \rangle \approx 0.5$ m/s with the present pipe section. In this work, the rotating velocity is half the maximum one, corresponding to a disc Reynolds number

$$Re_d = \frac{\langle V \rangle d}{\nu} \simeq 3.10^5, \tag{1}$$

for a kinematic viscosity $\nu = \mu/\rho$ taken at 2.32 K. A rough estimation of the Taylor microscale Reynolds number at the location of the probe can be made assuming an integral

TABLE II. Flow's main characteristics. Temperature is computed from the measured pressure of the saturated liquid. Densities and kinematic viscosity are computed using the temperature and pressure corrected from the hydrostatic pressure.

Temperature T (K)	Pressure P (mBar)	Superfluid fraction ρ_s/ρ (%)	Kinematic viscosity μ/ρ (m^2/s)
2.32	70	0	1.99×10^{-8}
2.15	47.3	11.3	1.52×10^{-8}
2.10	41.3	25	1.28×10^{-8}
1.95	26.9	51	9.57×10^{-9}
1.85	19.6	63	9.00×10^{-9}
1.55	6.08	85.8	9.50×10^{-9}
1.28	1.42	95.7	1.24×10^{-8}

scale of $d/2$ and a turbulence intensity of 7% (as measured), $R_\lambda = \sqrt{15 \times 0.07 V d/2\nu} \sim 400$.

Temperature is decreased below 4.2 K by pumping the helium bath with a roots group (Leybold model SV300 and WS2001). With such a flow, temperature can be as low as 1.28 K at the largest Reynolds numbers. This corresponds to a superfluid fraction of nearly 96% (see Table II). Experiments have been performed at seven different temperatures.

B. Instrumentation

1. Probes

Two probes, a micro-cantilever anemometer and a miniature total head-pressure probe (later referred to as the "Pitot tube"), are inserted in the test section.

The micro-machined cantilever is sketched in Fig. 2(a), above an electron microscope image. It consists in a rectangular beam, 375 μm long, 32 μm large, and 1.2 μm thick, made of silicon oxide which is deflected by the incident flow. Both probes are sensitive to the local dynamic pressure $\frac{1}{2}\rho u^2$. The cantilever beam, its supporting structure, and its built-in resistive strain gauge are machined using micro-system techniques in a clean room. Details about the manufacturing process can be found in Refs. 24 and 25. The first resonance frequency of the cantilever immerged in liquid helium is estimated to be around 5 kHz,[25,26] which is above the range of frequency of interest in the present study (typically DC-1 kHz).

The Pitot tube is built with a capillary tube of internal diameter 0.8 mm and 34 mm long, parallel to the mean flow at one end and closed with a micro-machined differential piezoresistive pressure transducer at the other end. The Helmholtz resonance of this probe at ambient temperature is close to 1500 Hz, leading to a 500 Hz resonance at 2 K, due to the threefold ratio between sound velocity in atmospheric air and in liquid helium. Unfortunately, acoustic perturbations have polluted the signal and significantly reduced the exploitable frequency range down to 70 Hz typically. As a consequence, we only use the Pitot tube to validate the mean response of the cantilever probe and the efficiency of the centrifugal pump, using the well-known quadratic response of Pitot tubes versus velocity.

Both miniature Pitot tubes and micro-cantilevers have been previously validated for anemometry of the longitudinal velocity component in wind-tunnels, above and below the superfluid transition.[5,10,24,27] In He-II, both anemometers are sensitive to the barycentric velocity of the superfluid and normal fluid $V = V_s\rho_s/\rho + V_n\rho_n/\rho$ (with obvious notation). But at the inertial scale resolved by the probes, the two fluids are known to be locked together in this temperature range,[28] and the probes are thus sensing the common velocity: $V \simeq V_s \simeq V_n$.

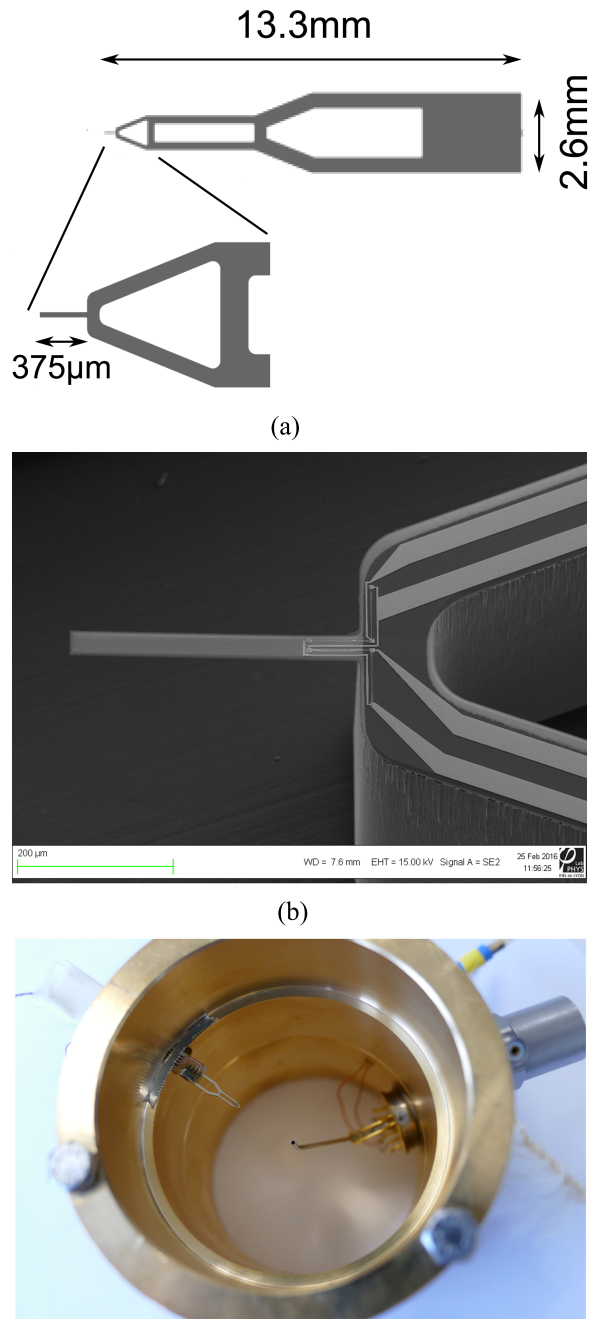

FIG. 2. Two probes were inserted in the wind tunnel: a Pitot tube and a micro-machined cantilever anemometer. (a) Sketch of a cantilever probe. (b) Electronic microscope image of the cantilever. (c) View of the probes.

2. Position in the flow

Reference 19 shows that wake turbulence downstream a disc becomes fully developed (i.e., self-similar) at 15 disc

diameters, for an unconfined flow with $Re_d \simeq 7.10^4$. In our experiment, Re_d is half a decade larger and the disc of diameter $d = 2.5$ cm is confined in a tube of diameter 5.1 cm, which obviously results in different streamwise flow properties. To our knowledge, no study of this particular issue in the wake of a disc and at such a large Reynolds number exists. Thus, we have chosen to place the probes 20 disc diameters downstream the disc of diameter d and we do not expect turbulence to be fully developed down to the smallest scales of the inertial range

The Pitot tube is located on the axis of the test section whereas the cantilever is $d/6$ aside the axis, see Fig. 2(c).

C. Measurement protocol

Two different electronic circuits are used: one dedicated to high signal-to-noise fluctuation measurements (see Fig. 3) and the second one to accurate measurements of mean values. Two 9 V batteries in series polarise the circuitry, and their common pole is grounded to the cryostat. Two similar resistors in series with the batteries allow tuning the polarisation voltage of the Wheatstone bridge integrated on the probe. The typical polarisation of the cantilever is 43.6 mV (≈90 μA) and 1 V (≈175 μA) for the Pitot tube. The output signal is amplified directly on the top of the cryostat, using a low-noise AC preamplifier (EPC1-B), then anti-alias filtered by a KEMO 4th order filter. The acquisition is performed with an 18-bit multi-channel card (National Instrument 6289). The cutoff frequency f_c of the filter is chosen to satisfy the Shannon criterion ($f_c < f_s/2$, with f_s as the sampling frequency). A numerical low-pass filter at 800 Hz further reduces the bandwidth to discard frequencies altered by the $0.7nV/\sqrt{Hz}$ noise floor, which is reached around 1 kHz and corresponds to the voltage noise of the preamplifier. In this configuration, the frequencies below ~10 mHz are rejected by the AC-preamplifier. That is why a dedicated DC electrical circuit is needed to measure the mean response of the probes. This is done replacing the batteries with a symmetrical 10 Hz AC source and performing lock-in detection (NF LI5640) on the pre-amplified output signal. Although neither signal distortion nor probe over-heating was found, as a precaution, the AC driving voltage is chosen to be equivalent to one of the circuits with batteries.

Calibration is performed *in situ* using the mean response curves and a quadratic fit of the mean signal versus rotating velocity of the propeller (see Fig. 4). This response is fully consistent with the one obtained in air.[25] It is then possible to reconstruct the complete signal of the probes by combining the AC and the DC measurements. Surely, AC frequencies below 10 mHz are not fully recovered with this procedure, but this has no consequence on the results of the present study.

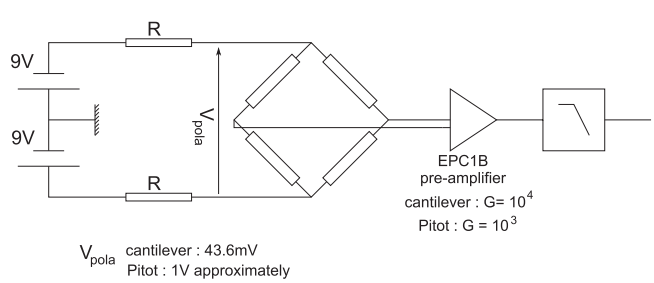

FIG. 3. Electrical circuit used for fluctuation acquisitions. The Wheatstone bridge is fully integrated on the probe. In the alternative circuit used to calibrate the DC response of the probe, the batteries are replaced by an AC symmetrical voltage generator, and the filter is replaced by the input of a lock-in amplifier synchronized to the AC generator.

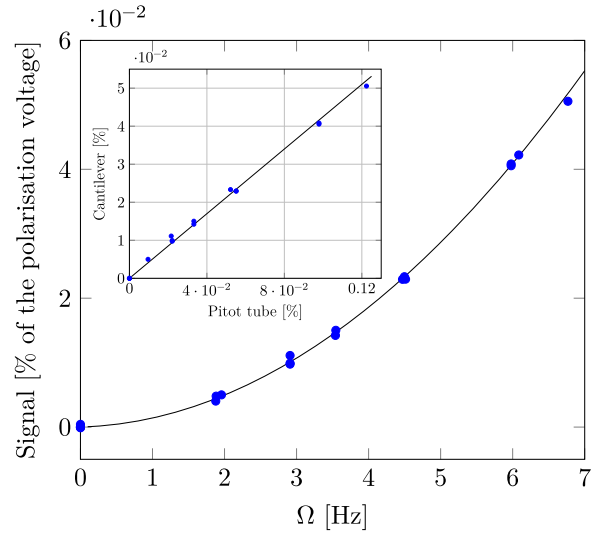

FIG. 4. Mean response of the cantilever probe versus the rotating velocity of the propeller, Ω, in (Hz). Ω can be considered as an image of the mean flow velocity at first order. The signal of the cantilever is quadratic versus velocity and linear versus signal of the Pitot tube (see the inset) as illustrated by the parabolic and linear fits.

1. Validation of the cantilever response

The cantilever beam is deflected by the hydrodynamic force imposed by the flow. As for the Pitot tube, this force is directly related to the dynamic pressure generated by the incoming flow. Above the superfluid transition, the typical Reynolds numbers based on the transverse size $l = 32$ μm for the cantilever is the following:

$$Re_{canti} = \frac{\langle V \rangle l}{\nu} \approx 450. \tag{2}$$

At such a large Reynolds number, the dynamical pressure scales with the square of the velocity $p = \rho V^2/2$.[29] The signal of the cantilever should then be quadratic with respect to the rotating velocity of the pump, which is actually the case (see Fig. 4), and linear with respect to the Pitot tube signal, as confirmed by the inset.

III. RESULTS AND DISCUSSIONS

A. Flow characterisation

Using the so-called Reynolds decomposition, velocity fluctuations are defined as

$$v = V - \langle V \rangle . \tag{3}$$

Figure 5 shows the probability density functions (PDF) of fluctuations in root mean square (noted RMS) units. All time series plotted are obtained for the same propeller rotation ($\Omega \approx 3.5$ Hz) and thus for nearly the same mean velocity. Colors correspond to different temperatures except for the 1.85 K temperature ($\rho_s/\rho = 63\%$), which has been achieved

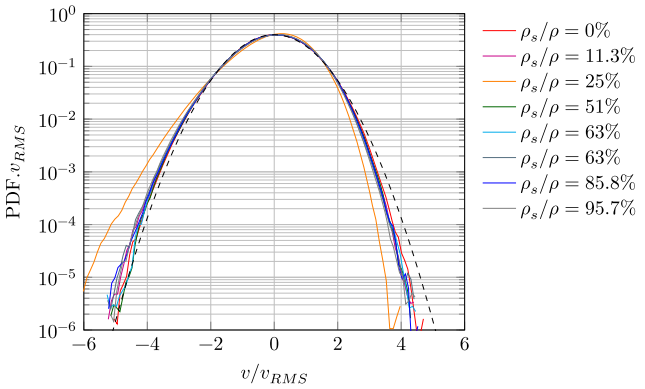

FIG. 5. PDF obtained at different mean temperatures and nearly constant mean velocity ($\Omega \approx 3.5$ Hz). The dashed line corresponds to a gaussian distribution.

twice and is represented using two different colors. Except the $\rho_s/\rho = 25\%$ time series (2.1 K), all the PDFs remain close to a gaussian, with a small residual dissymmetry [skewness $v^3/({v_{RMS}}^{3/2})$ within (−0.16; −0.11)]. This suggests that turbulence is not yet completely developed at 20 diameters downstream the disc. We have no explanation for the odd behavior of 2.1 K time series; one could speculate on the appearance of a flow instability producing a recirculation or a corner-flow near the disc. Unfortunately, we discovered this odd behaviour too late to repeat the measurements.

Frequency spectra are presented in Fig. 6. As previously said, the time series are numerically filtered at 800 Hz, which explains the corresponding cutoff. To improve this signal-to-noise ratio, a higher polarisation voltage would have been necessary. Unfortunately, higher polarisations have proved to be potentially destructive for the fragile micro-machined electrical tracks of the probe.

At low frequency (typically $f \lesssim 10$ Hz), the spectra evidence a characteristic plateau of one-dimensional velocity spectra. Above 10 Hz typically, the slope gets close to −5/3, which is characteristic for a fully developed turbulent cascade regime.[6] This slope has been reported in previous superfluid experiments in various very high Reynolds number

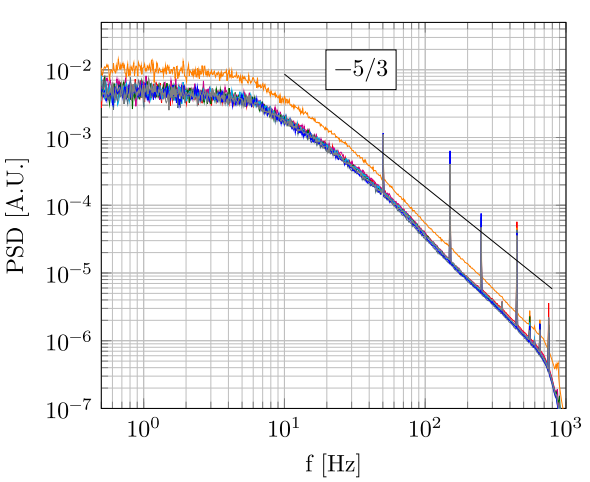

FIG. 6. Spectra of the velocity measured with the cantilever probe. The color code is the same as in Fig. 5. The cutoff at high frequency results from signal filtering.

flows, such as von Kármán cells,[10,30] wind tunnels,[31] disc wakes,[5] grid flows,[27] and jets.[32] A closer analysis shows that the slope becomes slightly steeper than −5/3 in the second half of the resolved inertial range (roughly above 140 Hz). This is consistent with an incomplete development of the turbulent cascade and consistent with the observations of Refs. 21 and 22 in the wake behind a disc with a classical flow in conditions compatible with the present ones. A peak compatible with the vortex shedding frequency could have been expected around 1 Hz typically, which is not the case here. Two explanations are possible. First, in an unconfined flow, the appearance of the peak is dependent on the radial position of the probe, in particular the peak can disappear at the center of the wake. Second, in some flows, the phenomena of vortex shedding are not present for specific ranges of the Reynolds number compatible with the present one, as shown by Ref. 33 in the wake of cylinders.

The spectrum associated with the 2.1 K time series differ from the others, again. Its spectrum is more energetic, which is consistent with the appearance of a large scale flow instability in the tunnel, feeding more energy in the cascade. Considering that our main interest is not in this range of superfluid density ratio, we will not exploit this temperature in the following. Since no difference was found between the two time series independently recorded at 1.85 K, only one will be displayed in the following figures.

As a test of data convergence, we examine third order statistics of velocity increments, which reveals the energy cascade process from large scales to small ones. The increments δv of the longitudinal velocity V in the x direction parallel to the mean flow are defined as

$$\delta v = V(x + \delta x) - V(x). \tag{4}$$

Taylor's frozen turbulence hypothesis is used to map the time domain, where the time series $V(t)$ are acquired, to the space domain $V(x)$, where the velocity increments are defined. This mapping is justified by the low turbulent intensity of the present flow, close to 7%. Using one of the datasets, we checked that the use of the instantaneous Taylor hypothesis[34] was not changing significantly the intermittency exponents (and only slightly accounting for the residual velocity skewness). The negligible influence on scaling exponents of this improved Taylor hypothesis was already pointed in the original paper.[34] In practice, velocity increments will be directly estimated in the time domain as

$$\delta v = V(t) - V(t + \tau) \tag{5}$$

with $\tau = \delta x / \langle V \rangle$. The 4/5 law of turbulence predicts the inertial-range scaling of the skewness of velocity increments,

$$\left\langle \delta v^3 \right\rangle = -\frac{4}{5} \epsilon \cdot \delta x = -\frac{4}{5} \epsilon \langle V \rangle \tau, \tag{6}$$

where $\langle \cdots \rangle$ denotes time averaging. At the Reynolds number of the present study ($R_\lambda \sim 400$), one does not expect a well defined plateau when plotting $\left\langle \delta v^3 \right\rangle / \tau$ versus τ due to finite Reynolds number corrections. The 4/5 prefactor itself (not measurable in our experiment due to calibration uncertainty) is expected to be only approximatively reached (typ. within 10%) in the middle of the inertial range

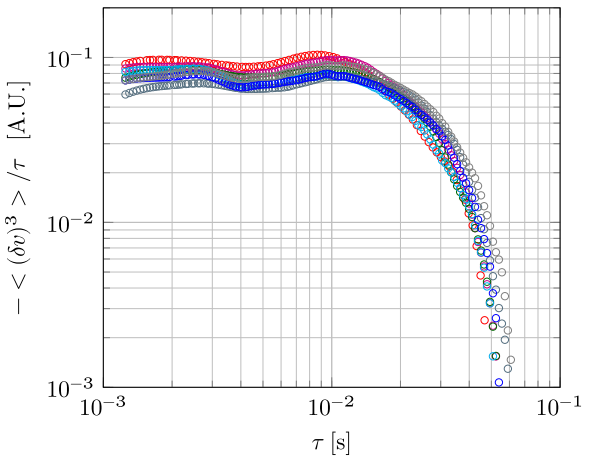

FIG. 7. Third order structure function, same color code as in Fig. 5.

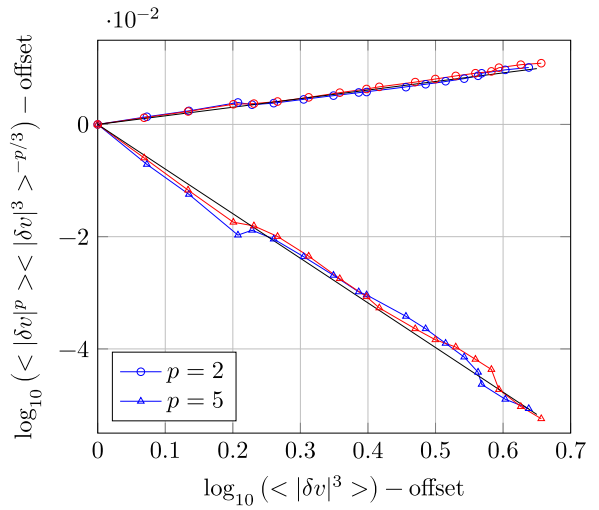

FIG. 8. Example of the determination of the intermittency correction $\mu_p = p/3 - \zeta_p$ (here at 2.32 K for the blue curves and 2.15 K for the red ones). In this representation, the mean slope of each set of points is $-\mu_p$. The time increments are windowed in the frequency range 20–140 Hz. Black lines are the fit of the 2.32 K case.

(e.g., see Refs. 36 and 37 and reference within). With this in mind, one can still distinguish in Fig. 7 a clear leveling of this compensated third moment in the inertial range, which is consistent with the literature (for example, see Refs. 35 and 38) even if we do not resolve the small scales where $\langle \delta v^3 \rangle$ is expected to decrease to 0.

B. Determination of intermittency exponents

There exist several ways to quantify intermittency and this topic is still debated (e.g., see discussion in Ref. 8). The motivation of the present work is not to obtain *absolute precision* in the coefficient characterizing intermittency but rather to obtain *sensitivity* in the determination of these coefficients versus temperature. This motivated the choice of a wake flow and led us to use the so-called "extended self similarity" (ESS) method[39] to quantify intermittency through a set of scaling exponents ζ_p defined in the (extended) inertial range as

$$\langle |\delta v|^p \rangle \sim \left(\langle |\delta v|^3 \rangle \right)^{\zeta_p}. \tag{7}$$

This method produces extended scaling ranges, which allows an accurate determination of the exponents ζ_p. One drawback of this method is the (small) difference between the ESS exponents ζ_p and the exponents ζ'_p resulting from the "genuine" definition $\langle \delta v^p \rangle \sim \delta x^{\zeta'_p}$. This drawback is *a priori* not an issue here since we focus on the relative *variation* of exponents versus temperature. We will come back on this point in Sec. IV.

As a preliminary test of statistical convergence, we computed the histograms of $|\delta v|^p$ up to $p = 6$ and checked that their tails well converge to zero. To determine the ESS exponents ζ_p, we focus on their deviation from the exponents $p/3$ that would be expected in the absence of intermittency. Thus, the *intermittency corrections* $\mu_p = p/3 - \zeta_p$ are directly fitted using a compensated log-log plot of $\langle |\delta v|^p \rangle \langle |\delta v|^3 \rangle^{-p/3}$ versus $\langle |\delta v|^3 \rangle$ or more precisely $-\mu_p$ is fitted as the slope of the affine function,

$$\log\left(\frac{\langle |\delta v|^p \rangle}{\langle |\delta v|^3 \rangle^{p/3}} \right) = -\mu_p \cdot \log(\langle |\delta v|^3 \rangle) + cst. \tag{8}$$

This fit was performed for time increments chosen within 0.007-0.05 s (i.e., 20-140 Hz), a range of increments which avoids the highest frequency part of the spectrum where the cascade is not fully developed. Although this range of increment is limited to 0.84 decade, the good statistical converge of the data allows an accurate determination of a local exponent μ_p, as illustrated by Fig. 8. This accurate determination should also be credited to the ESS method, which partly compensates for the absence of a pure scaling over the spectral range 20-140 Hz. As a check, a reduced range of time increments (20-80 Hz) will also be used. The small steps visible for the $p = 5$ datasets of Fig. 8 are also present for the other orders and are interpreted as noise. In this representation, they do not alter significantly the slope determination and therefore exponent determination. They would have been more detrimental if we were estimating exponents using the derivative $d \log \langle |\delta v|^p \rangle / d \log(\langle |\delta v|^3 \rangle)$ and that is why we did not use this alternative approach.

All the structure function exponents ζ_p and their fitting uncertainties are reported in Table III and plotted in Fig. 9. The error bars associated with the uncertainties are too small to worth plotting in Fig. 9 and later figures. The exponents derived from Kolmogorov's 1941 self-similarity arguments (absence of intermittency, $\zeta_p = p/3$) and those from the She-Lévêque model[40] ($\zeta'_p = \frac{p}{9} + 2[1 - (\frac{2}{3})^{p/3}]$) are plotted for comparison. A direct quantitative comparison with the later model is delicate due to our use of the ESS method and the lack of isotropy and homogeneity of wake flows, but we can state that

TABLE III. Structure function exponents calculated with the ESS method in the 20-140 Hz range.

T (K)	$\zeta_1 \pm 0.2$ (%)	$\zeta_2 \pm 0.1$ (%)	$\zeta_4 \pm 0.2$ (%)	$\zeta_5 \pm 0.5$ (%)	$\zeta_6 \pm 0.7$ (%)
2.32	0.349	0.682	1.302	1.585	1.86
2.15	0.350	0.683	1.301	1.59	1.86
1.95	0.349	0.683	1.300	1.585	1.85
1.85	0.348	0.681	1.303	1.59	1.86
1.55	0.348	0.681	1.304	1.595	1.87
1.28	0.348	0.682	1.303	1.59	1.87

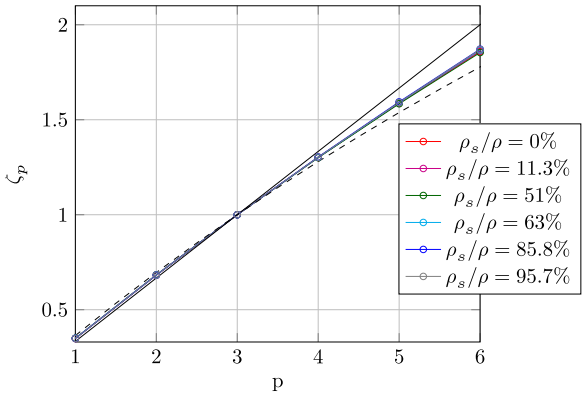

FIG. 9. Experimental exponents computed using the ESS method (coloured circles). The error bars corresponding to the fit uncertainty reported in Table III are not plotted because they are smaller than the size of the circle symbols. For comparison, exponents $\zeta_p = p/3$ expected with no intermittency (black line) and those from the She-Lévêque model[40] ($\zeta'_p = \frac{p}{9}+2[1-(\frac{2}{3})^{p/3}]$) are also plotted, predicted using the standard definition of exponents (dashed curve).

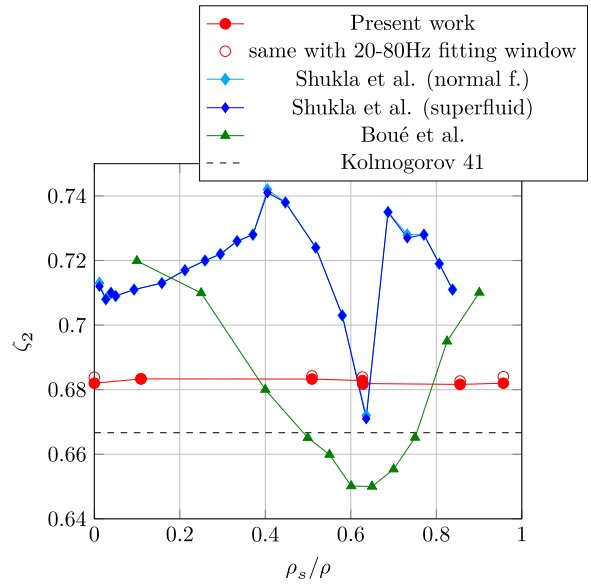

FIG. 10. Exponents of the second order structure function as a function of the superfluid fraction. For explanation on open symbols, see the text.

the flow presents the characteristic features of intermittency (e.g., $\mu_2 < 0$ and $\mu_4, \mu_5, \mu_6 > 0$) and is quantitatively consistent with previous velocity fluctuation measurements done using a miniature Pitot tube in a perfectly homothetic confined wake geometry.[11]

The main result of this study is the following: up to uncertainties and over the full temperature range explored, intermittency is found independent from the superfluid fraction, including the intermediate temperature cases where a pronounced temperature dependence was reported in some numerical studies.[12,14]

C. Comparison with previous studies

A preliminary comment is needed before comparing the exponent ζ_p from experiment and numerics. Since the anemometer is sensing (one component of) the barycentric velocity $V = V_s\rho_s/\rho + V_n\rho_n/\rho$, the experimental exponents ζ_p are therefore characterizing this specific velocity. In shell-model simulations, the normal fluid and superfluid velocity fields are modeled separately by discrete complex variables u_m^n and u_m^s, one for each shell of index m (wavelength). Exponents are therefore computed separately for each fluid component. Still, due to the strong coupling between the two fluids, they are nearly locked together in the inertial range ($V_s \simeq V_n \simeq V$), which implies that the normal and superfluid exponents are similar. This is indeed the case in the numerics as illustrated in Fig. 10, in the supplemental materials of Ref. 14 (see the G1-G21 subsets, which are obtained using the fluid properties of He-II), and in Fig. 1 of Ref. 12 which shows similar normal and superfluid structure functions in the inertial range, implying similar intermittency exponents. It is therefore fair to compare the exponents from the experiment and numerics. Surely, this would no longer be straightforward if we were studying small-scale intermittency and not inertial-range intermittency.

To summarize the existing results, experiments (Refs. 10 and 11 and present study) and simulations (Refs. 11, 12, and 14) did not reveal any difference of intermittency between classical turbulence and quantum turbulence in both temperature limits: high ($\rho_s/\rho \ll 1$) and low (but finite) temperatures ($0.04 \lesssim \rho_n/\rho \ll 1$). In the intermediate temperature range, the present experiment exhibits no difference between the classical and quantum cases up to an excellent resolution, in contradiction with shell-model simulations predicting significant enhancement[12] or reduction.[14]

To illustrate quantitatively the disagreement between our experiment and both shell simulations, we plot in Fig. 10 the second order exponent ζ_2 from these three studies. The values in the classical (Navier-Stokes) limit $\zeta_2^{NS} = \zeta_2(\rho_s = 0)$ differ between the shell models (0.72) and our experiment results ($\simeq$0.68) but this should not be considered as an issue. Indeed, the absolute value of ζ_2^{NS} results from an arbitrary choice of model parameters in shell simulations (as recalled in Ref. 12) and it is biased by the use of the ESS method in experiments, as already explained, and possibly by residual non-homogeneity and anisotropy of wake flows. To check if the 20-140 Hz windowing of the time increments as a significant impact of the fitted exponents, the reduced window 20-80 Hz was also used. The open symbols in Fig. 10 show that the impact is limited. The most striking features of this figure are the difference in temperature dependence between the three studies. Interestingly, the exponents ζ_2 obtained in the simulations by Shukla and Pandit[14] both exceed and fall short of their classical limit ζ_2^{NS}, which could be interpreted, respectively, as an intermittency enhancement and reduction. In Boué *et al.* simulations,[12] the exponents ζ_2 have a minimum below the Kolmogorov 1941 value $\zeta_2 = 2/3$, which corresponds itself to the absence of intermittency. The authors' interpretation of an "enhancement" of intermittency (instead of the apparent cancellation) is based on higher order exponents.

To focus on the possible superfluid effect on the intermittency, we now consider the relative exponents,

$$\zeta_p - \zeta_p^{NS} = \zeta_p - \zeta_p(\rho_s = 0) \simeq \zeta_p - \zeta_p(\rho_s \to 0), \qquad (9)$$

which can be seen as the superfluid correction to the classical exponent. Since all studies agree that the classical exponents

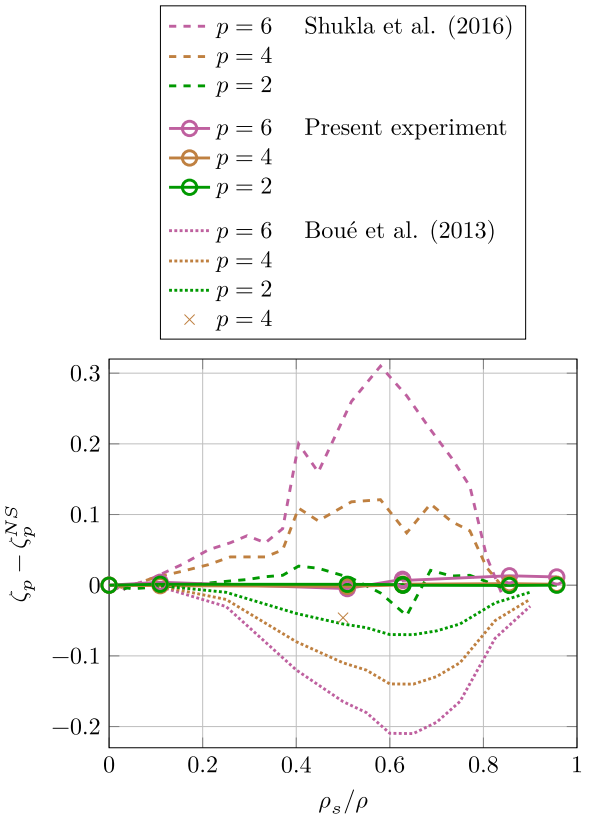

FIG. 11. Superfluid correction of the intermittency exponents. Note that the dotted line for orders $p = 4$ and $p = 6$ have been calculated from an analytical formula provided in the original paper.

ζ_p^{NS} are recovered in the $\rho_s/\rho \to 0$ limit, this definition allows us to single out only superfluid effects.

Figure 11 represents this superfluid intermittency correction on exponents for $p = 2, 4, 6$. To put numbers on Eq. (9), values from Shukla and Pandit simulations are taken from the supplemental materials of their article.[14] Boué *et al.* paper[12] provides one value $\zeta_4 \simeq 1.21$ for $\rho_s/\rho = 0.5$ and $\zeta_4^{NS} = 1.256$ (see cross in Fig. 11), a plot of ζ_2 and a relation for ζ_p versus ζ_p^{NS} and ζ_2 "in good agreement with the observed values" [with our notations, they found $\zeta_p - \zeta_p^{NS} = p\left(\zeta_2 - \zeta_2^{NS}\right)/2$] which allowed us to estimate the complete Fig. 11. Similarly to Fig. 10, the differences between the three studies are striking: no superfluid effect is found in the present experiment, while strong opposite effects are reported in the shell simulations. This is the central experimental result of this study.

IV. CONCLUDING REMARKS

We measured intermittency in the upper inertial range of a turbulent cascade of superfluid ^{4}He, with a special attention for the intermediate temperatures where none of the two fluid components of He-II can be neglected. In this range of temperature, no other experimental data were published and two published simulations are giving contradictory results: Boué *et al.* predicting an excess of intermittency[12] and Shukla and Pandit a deficit of it.[14] Our measurements disagree with both simulations: we do not detect any temperature dependence of scaling exponents (with better than ±0.7% precision up to 6th order) when the temperature is varied between the Navier-Stokes limit ($\rho_s = 0$ for $T = 2.32$ K) down to 1.28 K, where 96% of He-II is superfluid. Our results also contradict a LES claiming an enhancement of intermittency near 1.6 K.[15]

Understanding the reason for the disagreements between the shell-model simulations[12,14] is beyond the scope of this paper. As acknowledged by the authors of these numerics, it is not surprising that shell-model simulations recover the classical intermittency exponents in the low and high temperature limits. Indeed, in these limits, the fluid with the largest density fully controls the dynamics without being significantly disturbed by the low-density one (which follows the former due to strong coupling). Thus, one recovers a one-fluid dynamical system with an inter-shell coupling term $NL[u_m^{n,s}]$ and numerical coefficients "a, b, c" which had been specially tuned to recover the classical exponents. The disagreement between both simulations (not to mention the experiment) at intermediate temperatures question the ability of the traditional inter-shell-coupling model to capture the intermittent corrections in the presence of mutual coupling between the superfluid and normal fluid, at least for the mutual coupling model implemented in both simulations. To go beyond, a systematic study of the sensitivity of scaling exponents versus shell-model parameters could be interesting. Further studies in particular high-resolution DNSs will probably be of great help. Efforts in this direction are underway by different groups.

We now come back to the comparison between the shell-model simulations and the experiments. The simulations provide the *absolute* scaling exponents ζ_p' defined as $\langle|\delta u_m|^p\rangle \sim k_m{}^{-\zeta_p'}$ (k_m is the wavevector of the mth shell), which is the shell-model version of the definition $\langle|\delta v|^p\rangle \sim \delta x^{\zeta_p'}$. The ESS method used for the experiment produces *relative* scaling exponents ζ_p [see Eq. (7)] defined with respect to the third moment, which is expected to scale linearly with δx in the inertial range of homogeneous isotropic turbulence. It has been noticed that (inertial range) absolute exponents ζ_p' determined from shell-model simulations can be sensitive to the dissipative processes occurring at small scales, while relative exponents $\zeta_p \sim \zeta_p'/\zeta_3'$ are not.[41] *A priori*, this could have explained the observed discrepancy between the experiment and shell-model, but it is not the case here, as can be seen in two ways. First, if the absolute exponents of ζ_2' in the present study had the 10% temperature dependence found in the simulations, the spectra of Fig. 6 would not overlap as well. Second, when the absolute exponents reported in the shell-model simulations[12,14] are normalized by the third order exponent, we find that ζ_p'/ζ_3' still have a significant temperature dependence. Thus, the difference of definition of scaling exponents cannot explain the qualitative difference between these simulations and the experiment.

On the experimental side, it would be interesting to extend the result to purely homogeneous and isotropic conditions. The use of a grid to generate turbulence would have produced a more "ideal" flow, but also smaller length scales and a smaller level of velocity fluctuations, resulting in a significantly lower range of resolved scales given to finite resolution and sensitivity of probes. New probe and flow designs would therefore be required to go in this direction. Regarding the

present results, we only explored the inertial range over nearly 1 decade of scales (the largest ones) and we cannot exclude that a different picture may emerge at smaller scales. In particular, it would be interesting to explore length scales closer to the mesoscale "gray" zone, where strong differences in the dynamics between the superfluid and normal fluid are expected to appear and a partial randomization (or equipartition) of the superfluid excitations has been predicted.[42]

ACKNOWLEDGMENTS

We thank G. Garde for the mechanical design and realization of the experimental apparatus, E. Verloop for the pumping group electrical control system, and G. Bres for the specific liquid helium level electronics. We are also grateful to F. Chillà and B. Castaing for their participation in the design of the cantilever, Y. Gagne, E. Lévêque, and T. Dombre for sharing their insights on intermittency and shell models, and B. Hébral for his feed-back. We acknowledge financial support from EC Euhit Project (No. WP21), which enabled the development of probes, financial support from the ANR SHREK for the pumping group, and support from the ANES.

[1] R. J. Donnelly, *Quantized Vortices in Helium-II*, Cambridge Studies in Low Temperature Physics (Cambridge University Press, Cambridge, 1991).
[2] S. W. Van Sciver, *Helium Cryogenics*, International Cryogenics Monograph Series (Springer, 2012).
[3] C. F. Barenghi, L. Skrbek, and K. R. Sreenivasan, "Introduction to quantum turbulence," Proc. Natl. Acad. Sci. U. S. A. **111**(Suppl. 1), 4647–4652 (2014).
[4] C. F. Barenghi, V. S. L'vov, and P.-E. Roche, "Experimental, numerical, and analytical velocity spectra in turbulent quantum fluid," Proc. Natl. Acad. Sci. U. S. A. **111**(Suppl. 1), 4683–4690 (2014).
[5] J. Salort *et al.*, "Energy cascade and the four-fifths law in superfluid turbulence," Europhys. Lett. **97**, 34006 (2012).
[6] U. Frisch, *Turbulence: The Legacy of A. N. Kolmogorov* (Cambridge University Press, 1995).
[7] K. R. Sreenivasan and R. A. Antonia, "The phenomenology of small-scale turbulence," Annu. Rev. Fluid Mech. **29**, 435 (1997).
[8] A. Tsinober, *The Essence of Turbulence as a Physical Phenomenon: With Emphasis on Issues of Paradigmatic Nature* (Springer Science & Business Media, 2013).
[9] R. Benzi and L. Biferale, "Homogeneous and isotropic turbulence: A short survey on recent developments," J. Stat. Phys. **161**(6), 1351–1365 (2015).
[10] J. Maurer and P. Tabeling, "Local investigation of superfluid turbulence," Europhys. Lett. **43**, 29 (1998).
[11] J. Salort, B. Chabaud, E. Lévêque, and P. E. Roche, "Investigation of intermittency in superfluid turbulence," J. Phys.: Conf. Ser. **318**, 042014 (2011).
[12] L. Boué *et al.*, "Enhancement of intermittency in superfluid turbulence," Phys. Rev. Lett. **110**, 014502 (2013).
[13] L. Biferale, "Shell models of energy cascade in turbulence," Annu. Rev. Fluid Mech. **35**(1), 441–468 (2003).
[14] V. Shukla and R. Pandit, "Multiscaling in superfluid turbulence: A shell-model study," Phys. Rev. E **94**, 043101 (2016).
[15] M. Bakhtaoui and L. Merahi, "Analysis of the energy budget in quantum turbulence: HVBK model," J. Low Temp. Phys. **178**, 129–141 (2015).
[16] G. Krstulovic, "Grid superfluid turbulence and intermittency at very low temperature," Phys. Rev. E **93**, 063104 (2016).
[17] E. Rusaouen, B. Rousset, and P.-E. Roche, "Detection of vortex coherent structures in superfluid turbulence," Europhys. Lett. **118**, 14005 (2017).
[18] H. Kahalerras, Y. Malecot, Y. Gagne, and B. Castaing, "Intermittency and Reynolds number," Phys. Fluids **10**, 910 (1998).
[19] T. Carmody, "Establishment of the wake behind a disk," J. Basic Eng. **86**, 869 (1964).
[20] S. Cannon, F. Champagne, and A. Glezer, "Observations of large-scale structures in wakes behind axisymmetric bodies," Exp. Fluid. **14**, 447 (1993).
[21] P. B. V. Johansson, W. K. George, and S. H. Woodward, "Proper orthogonal decomposition of an axisymmetric turbulent wake behind a disk," Phys. Fluid. **14**, 2508 (2002).
[22] P. B. V. Johansson, S. H. Woodward, and W. K. George, "The far downstream evolution of the high-Reynolds-number axisymmetric wake behind a disk. Part 1. Single-point statistics," J. Fluid Mech. **555**, 363 (2006).
[23] R. D. Mehta and P. Bradshaw, "Design rules for small low speed wind tunnels," Aeronaut. J. **83**, 443–453 (1979).
[24] J. Salort, P. E. Roche, and A. Monfardini, "Cantilever anemometer based on a superconducting micro-resonator: Application to superfluid turbulence," Rev. Sci. Instrum. **83**, 125002 (2012).
[25] J. Salort *et al.*, "Joint temperature and velocity local sensor for turbulent flows," Rev. Sci. Instrum. (submitted).
[26] J. E. Sader, "Frequency response of cantilever beams immersed in viscous fluids with applications to the atomic force microscope," J. Appl. Phys. **84**, 64–76 (1998).
[27] J. Salort *et al.*, "Turbulent velocity spectra in superfluid flows," Phys. Fluids **22**, 125102 (2010).
[28] P.-E. Roche, C. F. Barenghi, and E. Leveque, "Quantum turbulence at finite temperature: The two-fluids cascade," Europhys. Lett. **87**(5), 54006 (2009).
[29] S. F. Hoerner, *Fluid-Dynamic Drag: Practical Information on Aerodynamic Drag and Hydrodynamic Resistence* (Hoerner Fluid Dynamics, 1965).
[30] B. Rousset, P. Bonnay, P. Diribarne, A. Girard, J. M. Poncet, E. Herbert, J. Salort, C. Baudet, B. Castaing, L. Chevillard, F. Daviaud, B. Dubrulle, Y. Gagne, M. Gibert, B. Hébral, T. Lehner, P.-E. Roche, B. Saint-Michel, and M. Bon Mardion, "Superfluid high Reynolds von Kármán experiment," Rev. Sci. Instrum. **85**, 103908 (2014).
[31] P.-E. Roche, P. Diribarne, T. Didelot, O. Français, L. Rousseau, and H. Willaime, "Vortex density spectrum of quantum turbulence," Europhys. Lett. **77**, 66002 (2007).
[32] D. Durì, C. Baudet, J.-P. Moro, P.-E. Roche, and P. Diribarne, "Hot-wire anemometry for superfluid turbulent coflows," Rev. Sci. Instrum. **86**(2), 025007 (2015).
[33] P. W. Bearman, "On vortex shedding from a circular cylinder in the critical Reynolds number regime," J. Fluid Mech. **37**, 577 (1969).
[34] J.-F. Pinton and R. Labbé, "Correction to the Taylor hypothesis in swirling flows," J. Phys. II **4**, 1461–1468 (1994).
[35] R. A. Antonia, T. Zhou, and J. P. Romano, "Small-scale turbulence characteristics of two-dimensional bluff body wakes," J. Fluid Mech. **459**, 67 (2002).
[36] J. Qian, "Slow decay of the finite Reynolds number effect of turbulence wakes," Phys. Rev. E **60**, 3409–3412 (1999).
[37] R. A. Antonia and P. Burattini, "Approach to the 4/5 law in homogeneous isotropic turbulence," J. Fluid Mech. **550**, 175 (2006).
[38] F. Coscarella, S. Servidio, D. Ferraro, V. Carbone, and R. Gaudio, "Turbulent energy dissipation rate in a tilting flume with a highly rough bed," Phys. Fluids **29**, 085101 (2017).
[39] R. Benzi *et al.*, "Extended self-similarity in turbulent flows," Phys. Rev. E **48**, R29 (1993).
[40] Z.-S. She and E. Lévêque, "Universal scaling laws in fully developed turbulence," Phys. Rev. Lett. **72**, 336 (1994).
[41] E. Leveque and Z.-S. She, "Viscous effects on inertial range scalings in a dynamical model of turbulence," Phys. Rev. Lett. **75**, 2690–2693 (1995).
[42] J. Salort, P.-E. Roche, and E. Lévêque, "Mesoscale equipartition of kinetic energy in quantum turbulence," Europhys. Lett. **94**, 24001 (2011).